Available online at www.sciencedirect.com
SCIENCE DIRECT
Journal of Catalysis 241 (2006) 235–242
JOURNAL OF CATALYSIS
www.elsevier.com/locate/jcat

Ceramic microreactors for on-site hydrogen production

Christian [a], M. Mitchell [a], D.-P. Kim [b], P.J.A. Kenis [a,*]

[a] *Department of Chemical & Biomolecular Engineering, University of Illinois at Urbana-Champaign, 600 S. Mathews Ave., Urbana, IL 61801, USA*
[b] *Department of Fine Chemical Engineering & Chemistry, Chungnam National University, Daejeon, 305-764, South Korea*

Received 19 January 2006; revised 6 April 2006; accepted 8 April 2006

Available online 5 June 2006

Abstract

This paper describes the synthesis and characterization of ceramic microreactors composed of inverted beaded silicon carbide (SiC) monoliths with interconnected 0.75-, 2.2-, or 7.2-μm pores as catalyst supports, integrated within high-density alumina reactor housings obtained via an optimized gel-casting procedure. Structural characterization revealed that these tailored macroporous SiC porous monoliths are stable at temperatures up to at least 1200 °C, and have surface areas and porosities as high as 7.4×10^7 m^2/m^3 and 74%, respectively. Further characterization of the ceramic microreactors using the decomposition of ammonia with Ru as the catalyst at temperatures between 450 and 1000 °C showed that as much as 54 sccm of hydrogen, or 9.8×10^4 sccm H_2 per cm^3 of monolith volume, could be obtained from a 36-sccm entering stream of NH_3 at >99.9% conversion at temperatures above 700 °C. Moreover, using SiC as a catalyst support appears to increase the catalytic activity of the Ru catalyst, as evidenced by high turnover frequencies.

Keywords: Ceramic microreactor; Silicon carbide; Hydrogen production; Ammonia decomposition; Fuel reforming

1. Introduction

The continuous operation of electronic devices lacking access to wired electrical power, such as vehicles and electrical equipment in remote locations (e.g., construction sites, military fields), requires electrical power sources of high specific energy. Rechargeable lithium ion batteries are presently used for many of these applications, but they have energy densities of only up to ∼200 W-h/l and thus must be recharged frequently [1]. Higher energy densities can be obtained by using hydrogen gas in polymer electrolyte membrane (PEM) fuel cells [2–4]. The transport and storage of compressed hydrogen entails safety issues, however. By producing H_2 on-site [5,6] by, for example, decomposition of ammonia (energy density of ∼4 kW-h/l) or steam reforming of liquid hydrocarbons such as gasoline (energy density of ∼9 kW-h/l), fuel cells can provide electrical power for longer periods and have a higher specific energy than rechargeable batteries [2].

The decomposition of NH_3 within a microreactor is a direct route to producing H_2 for PEM fuel cells. The only products are H_2 and N_2, and this microreactor can be integrated with a microscale heat source, such as a microburner [7] or a catalytic combustor [8], making it advantageous for portable power applications due to the small overall volume. Compared to steam reforming of liquid hydrocarbons, the decomposition of NH_3 has fewer issues. Steam generation is not necessary, and no CO is produced; therefore, additional water–gas shift reactors and preferential oxidation reactors are not needed to avoid CO poisoning of the fuel cell catalyst [9]. Furthermore, the potential for sulfur poisoning of the reforming catalyst is avoided, eliminating the need for sulfur removal units or sulfur-tolerant catalysts [9]. A limitation still exists because NH_3 can poison the catalyst used in PEM fuel cells; however, an NH_3 adsorbent can be used to reduce the ammonia concentration to ppb levels on entering a PEM fuel cell [10].

Several microreactors for on-site production of H_2 have been reported [1,2,11–15]. Channel and posted reactors fabricated from anodized aluminum have been used for the decomposition of NH_3 up to 650 °C [11–13]. Integrated reformer systems consisting of burner, vaporizer, and reformer units have

* Corresponding author. Fax: +1 217 333 5052.
E-mail address: kenis@uiuc.edu (P.J.A. Kenis).

0021-9517/$ – see front matter
doi:10.1016/j.jcat.2006.04.033

been fabricated of stainless steel for the steam reforming of methanol between 260 and 450 °C [1,2,14]. In addition, MEMS fabrication methods have been used to produce silicon-based microreactors for methanol reforming [15]. Although these microreactor systems have achieved high conversion of NH_3 and methanol into hydrogen, they are often not stable for continuous operation above 800 °C, the minimum temperature required to eliminate coking of the catalyst during the steam reforming of higher hydrocarbons, such as propane and gasoline [16]. Aluminum melts at 660 °C, and silicon and stainless steel oxidize in the presence of steam above 800 °C and can corrode to a significant extent. Jensen et al. recently reported the more promising solution of a microreactor composed of suspended silicon nitride tubes with wash coats of catalyst to enable ammonia decomposition up to 825 °C [8].

To date, the development of high-surface area catalyst support structures that are stable above 800 °C has been a challenge, especially when the pressure drop across the support must be low enough to both reduce parasitic losses due to pumping of fluids and prevent mechanical failure of the structures. Recently, we have reported on the fabrication of inverted beaded monoliths with 7.2-μm interconnected pores, composed of silicon carbide (SiC) or silicon carbonitride (SiCN) [17], which are stable up to 1200 °C in air and have a ∼2 order of magnitude lower pressure drop than a packed beaded structure with the same geometric surface area. These monoliths also avoid the issues of cracking and channeling of the reactants, problems commonly encountered with wash coat-based catalyst layers and packed beds of loose catalyst particles.

In this paper, we describe the synthesis and characterization of ceramic microreactors composed of SiC catalytic monoliths with 0.75-, 2.2-, and 7.2-μm pores integrated in high-density alumina microreactor housings that we obtained using an optimized gel-casting procedure. We report a detailed analysis of the structural properties of the SiC catalyst supports (surface area, porosity, thermal stability) and of the deposited Ru metal on these supports (catalyst loading, dispersion, surface area of active sites). We further characterize these catalytic monoliths using the decomposition of ammonia into hydrogen and nitrogen at temperatures as high as 1000 °C, to show their promise in on-site hydrogen production for PEM fuel cells.

2. Experimental

2.1. Catalyst preparation

2.1.1. High-surface area porous monoliths (catalyst supports) preparation

Poly(dimethylsiloxane) (PDMS) molds with microchannel patterns were prepared for fabrication of porous monoliths and for molding of the high-density alumina housings (Section 2.3) by replica molding of a master obtained through photolithography [18]. For the preparation of SiC porous monoliths, we adopted the micromolding-in-capillaries (MIMIC) method used previously for the synthesis of porous oxide materials [19]. Solutions of polystyrene (PS) spheres (1.1, 3.2, and 10 μm diameter; Polysciences) were centrifuged three times at 10,000 rpm for 10 min (centrifuge 5415D, Eppendorf), with decanting of the water and addition of DI water after each centrifugation to remove surfactant. The final concentrated solution was obtained by removing half of the water after settling of the solution for 12 h. About 5–50 μL of the concentrated PS sphere solution was then placed at one end of a microchannel (500 μm wide, 150 μm high, 5–7 mm long) and left for 12 h for the completion of the packing process, followed by drying under vacuum at 70 °C for 48 h.

SiC porous monoliths were prepared by infiltration of the resulting packed beds of PS spheres in PDMS microchannels with a mixture of allylhydridopolycarbosilane (SP matrix, Starfire Systems) and 3–5 wt% of the thermal initiator 1,1-bis(*tert*-butylperoxy)-3,3,5-trimethylcyclohexane (92%, Aldrich), followed by curing of the precursor mixture at 70 °C for 12 h. All of these steps were carried out in a glove box under an argon atmosphere. After the PDMS mold was removed, pyrolysis was performed at 1200 °C for 2 h under an argon atmosphere, as described previously [17], to yield SiC porous monoliths typically 350 μm wide, 100 μm high, and 3 mm long after shrinkage, as shown in Fig. 1.

2.1.2. Catalyst deposition

Ruthenium (Ru) catalyst was deposited on the SiC porous monoliths by wet impregnation with 14.72 wt% (0.67 M) $RuCl_3$ (Aldrich) in a mixture of 10 vol% DI water in acetone, similar to a method described previously [11]. The structures were then dried in a conventional oven at 60 °C for 48 h to remove the remaining water and acetone, followed by calcination in air at 580 °C for 5 h using a tube furnace (HTF5500 series, Lindberg/Blue M). Finally, the catalyst was reduced in the tube furnace under an atmosphere of 5% H_2 in argon at 550 °C for 6 h.

2.2. Characterization of the porous catalytic monoliths

The morphology of the pores in the SiC porous monoliths was studied using either a Hitachi S-4700 or a JEOL 6060-LV scanning electron microscope. The surface areas of the SiC porous monoliths were determined by N_2 adsorption–desorption at 77 K using a BET apparatus (Micromeritics ChemiSorb 2705). Before the BET analysis, the samples were degassed under vacuum at 100 °C for 24 h to remove any moisture. Mercury intrusion porosimetry (MIP) analysis was carried out using a Micromeritics AutoPore II 9220 to determine the porosities of the SiC porous monoliths.

The dispersion of active metal phase of the Ru catalyst in the SiC porous monoliths was measured using pulsed CO chemisorption and H_2 chemisorption at room temperature using a Micromeritics ChemiSorb 2705, assuming a 1:1 ratio of CO or a 1:2 ratio of H_2 chemisorbed to exposed Ru metal. The Ru loading was determined using inductively coupled plasma spectrometry (OES Optima 2000 DV, Perkin–Elmer).

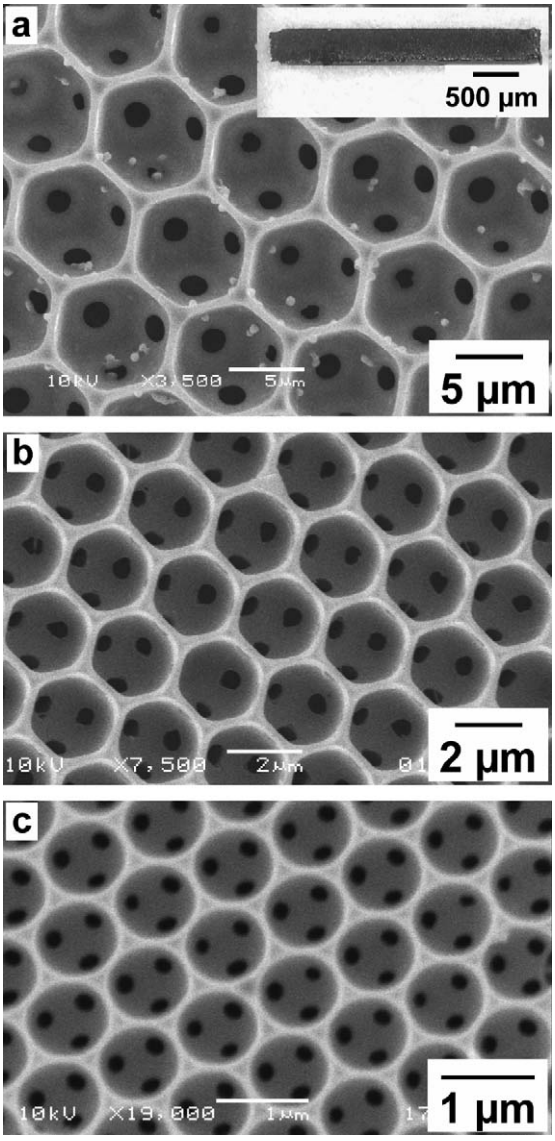

Fig. 1. SEM micrographs of fracture profiles of inverted beaded SiC monoliths after heating at 1200 °C for 6 h in air with (a) 7.2 µm pores (inset: an optical micrograph of the whole SiC porous monolith); (b) 2.2 µm pores; and (c) 0.75 µm pores. The black spots are the windows that connect adjacent pores in these close packed structures. The bits of debris are due to cutting of the samples before SEM analysis.

2.3. Fabrication of high-density alumina structures

The gel-casting forming method developed by Young et al. for mesoscale structures [20,21] was adapted here to enable the fabrication of cm-scale, high-density, nonporous alumina structures with submillimeter features for reactor housings and lids. High-purity alumina powder (Baikalox GE1, Baikowski) was initially deagglomerated using a jar mill (LABMILL-8000, Advanced Ceramics Research) containing milling media (99.9% alumina, Union Process) for 48 h. The weight ratio of alumina powder to milling media was 1 to 3.5. The powder was then mixed with monomer solution and dispersant, and milled further using the jar mill. The monomers, here methacrylamide (98%, Aldrich), N,N'-methylenebisacrylamide (99%, Aldrich), and 1-vinyl-2-pyrrolidinone (99%, Aldrich) in a 1.5:1:1.5 ratio by weight, were first dissolved in DI water to form a 20 wt% aqueous solution of monomers. The dispersant (Darvan 821A, R.T. Vanderbilt) was then added to the mixture in the amount of 2 wt% of the total powder used. A staged addition of powder to the mixture was required to obtain a ceramic slurry with a high alumina loading (here 50 vol%), as described previously [22]. The slurry was then separated from the milling media using a sieve, placed in an ice bath to prevent solvent evaporation, and degassed in a vacuum desiccator for up to 2 h to remove any air bubbles. N,N,N',N'-tetramethylethylenediamine (TEMED, 99%, Aldrich) and ammonium persulfate (APS, 99.99%, Aldrich) were added to the slurry (0.1 vol% of TEMED and 0.1 wt% of APS with respect to the monomer solution used), followed by stirring and deairing in a vacuum desiccator for 30 min while the slurry was placed in an ice bath.

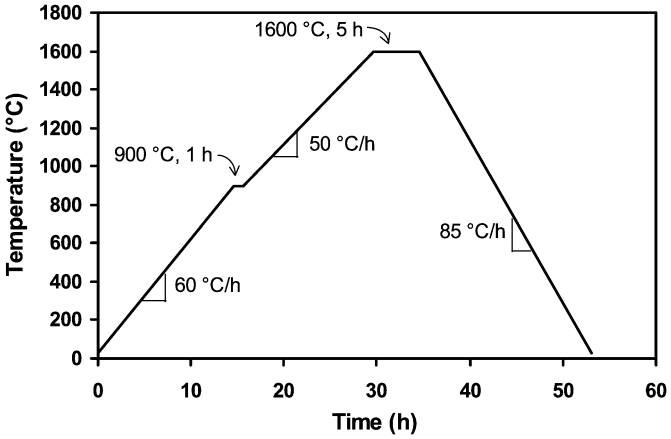

Fig. 2. Polymer removal and sintering temperature sequence used to obtain high-density, nonporous alumina housings and lids. The heating and cooling rates were optimized to avoid cracking and deformation in the final alumina structures.

The alumina slurry was then poured into PDMS molds with microchannel patterns (see Section 2.1.1) that were treated for 12 h with (tridecafluoro-1,1,2,2-tetrahydrooctyl)-1-trichlorosilane (United Chemical Technologies) after being cleaned by a plasma sterilizer (PDC-001, Harrick). Typical dimensions of the channels in the PDMS mold were 450 µm wide, 170 µm high, and 1.2 or 3.4 mm long; after shrinkage, the final channel dimensions were 400 µm wide, 150 µm high, and 1 or 3 mm long. After the slurry completely solidified in the mold due to catalytic polymerization of monomers, the resulting structures, the so-called "green bodies," were demolded and dried in a vacuum oven (5831 E series, Napco) at room temperature. The relative humidity inside the oven was initially maintained above 90% for 2 days, and then reduced by 10% every other day until 50% was reached. The green bodies were dried further under ambient conditions for two additional days. Debinding (i.e., removal of polymer) and sintering of the green bodies in a high-temperature furnace (1730 HT(c), CM furnaces) in air according to an optimized processing procedure (Fig. 2) yielded high-density, nonporous alumina structures: a microreactor design with slots for the placement of porous

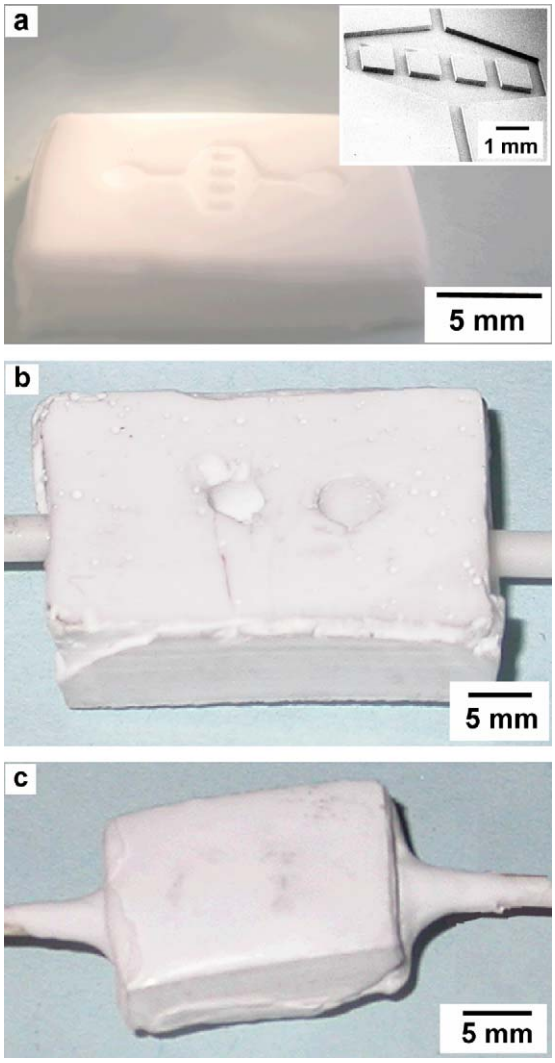

Fig. 3. (a) Optical and SEM (inset) micrographs of a high-density alumina housing with five microchannels (400 μm × 150 μm × 1 mm) in negative relief, obtained via gel-casting. Optical micrographs of (b) alumina lid and (c) assembled ceramic microreactor comprised of an alumina housing structure with five SiC porous monoliths (see Fig. 1), an alumina lid, and alumina inlet and outlet tubes.

monoliths and a lid with inlet holes as shown in Fig. 3. The polymer was completely removed during the initial stage of the thermal sequence (∼400–500 °C).

2.4. Assembly of integrated ceramic microreactors

After deposition of Ru catalyst, the SiC porous monoliths were mounted within the high-density alumina housing (see Fig. 3a) using ceramic paste (Ceramabond 569, Aremco Products). After applying the paste and inserting the monoliths into the microchannels, the housing was visually inspected under a stereozoom microscope (Leica, MZ 12.5, up to 30X) to ensure a good fitting of the monoliths within the channels. The alumina lid (see Fig. 3b) and alumina tubes (0.063 inch o.d. and 0.031 inch i.d.; CoorsTek) were then integrated with the housing using the same ceramic paste. After air-drying the paste at room temperature for 3 h, the integrated ceramic microreactor (see Fig. 3c) was placed in a tube furnace (HTF5500 series, Lindberg/Blue M) for final curing of the paste at 150 °C for 2 h in air.

2.5. Testing of the assembled ceramic microreactors

The flow of pure NH_3 (anhydrous, S.J. Smith) through the integrated ceramic microreactor was controlled using a mass flow controller (1479A MassFlo® Controller, MKS Instruments), and the temperature of the microreactor was controlled by placing it inside a tube furnace (HTF5500 series, Lindberg/Blue M). Reactants and products were led into and out of the ceramic microreactor through alumina tubes attached to stainless steel tubing outside of the tube furnace with Swagelok® connections. The conversion of NH_3 to H_2 and N_2 was measured using gas chromatography with a thermal conductivity detector (TRACE DSQ, Thermo Finnigan). Separations were performed using a Porapak N column (6 ft × 1/8 inch, stainless steel, 80/100 mesh; Fisher Scientific) with helium as the carrier gas. For each flow rate of pure NH_3, conversion data were obtained as a function of temperature by increasing the temperature of the furnace from 450 to 1000 °C in 50 or 100 °C increments. The average conversion and its standard deviation at a certain flow rate of NH_3 and temperature were calculated from at least three measurements after steady state was reached.

2.6. Determination of reaction rate constant

The rate constant at each temperature was determined using the plug-flow reactor (PFR) design equation for first-order kinetics with constant reactor temperature and a constant pressure gradient [Eq. (1)] and applying a weighted least squares method [23]. First-order kinetics are used to describe the decomposition of NH_3 based on earlier findings that at temperatures above 500 °C, the reaction becomes first order with respect to NH_3 and is not inhibited by H_2 [24,25],

$$v_0 \frac{(\Delta P + P_{\text{out}})}{(P_{\text{out}} + 0.5\Delta P)} = \frac{k' \text{SA}_{\text{active}}}{\{-X - 2\ln(1-X)\}} = k' \text{SA}_{\text{active}} y, \quad (1)$$

where v_0 is the inlet volumetric flow rate, k' is the rate constant in m/s, $\text{SA}_{\text{active}}$ is the surface area of active catalytic sites, ΔP is the pressure drop across the reactor (as calculated using the Ergun equation [26]), P_{out} is the pressure at the outlet of the reactor, and X is the conversion of NH_3. Equation (1) can be rewritten using $y = 1/\{-X - 2\ln(1-X)\}$; to determine the error in y (i.e., Δy) the following propagation of error equation was used:

$$\Delta y = (\partial y/\partial X)\Delta X. \quad (2)$$

With a weighted least squares analysis, the line of best fit passing through the origin was determined. The sum S in Eq. (3) was minimized as a function of the slope A of the line describing the $v_0(\Delta P + P_{\text{out}})/(P_{\text{out}} + 0.5\Delta P)$ versus y data,

$$S = \sum_i w_i \left[\left(v_0 \frac{(\Delta P + P_{\text{out}})}{(P_{\text{out}} + 0.5\Delta P)} \right)_i - A y_i \right]^2, \quad (3)$$

where w_i is equal to $1/(\Delta y)^2$. Once the value of A was determined, the rate constant was calculated using the relation $k' = A/\mathrm{SA}_{\mathrm{active}}$.

3. Results and discussion

3.1. Characterization of the porous catalytic monoliths

For the ammonia decomposition studies that we report here, we use inverted beaded SiC porous monoliths obtained following a procedure that we reported earlier for SiC and SiCN structures with 7.2-μm pores only [17]. In the work reported here, packed beds of PS spheres (1.1, 3.2, and 10 μm in diameter) were used as sacrificial templates for the synthesis of porous monoliths. Subsequent drying, infiltration with a preceramic polymer, curing, and pyrolysis yielded inverted beaded SiC porous monoliths with average pore diameters of 0.75, 2.2, and 7.2 μm, as determined from SEM micrographs (Fig. 1). We studied the chemical and physical stability of these SiC structures at high temperatures in an oxidative environment as described previously [17]. We compared the chemical composition (i.e., the fraction of silicon present as carbide, oxide, and oxycarbide) via X-ray photoelectron spectroscopy (XPS) and the pore morphology via SEM of the structures that were just prepared by pyrolysis under an argon atmosphere and after subsequent exposure to air at 1200 °C for 6 h. As before, XPS analysis of structures before and after thermal treatment in air showed a constant oxide content of ∼10–20%, and SEM micrographs showed that the morphology of the pores did not change on heating in air.

The *calculated* geometric surface areas of these monoliths based on pore diameters of 0.75, 2.2, and 7.2 μm were 5.9×10^6, 2.0×10^6, and 6.2×10^5 $\mathrm{m}^2/\mathrm{m}^3$, respectively. Using BET analysis, we determined *actual* surface areas of 7.4×10^7 $\mathrm{m}^2/\mathrm{m}^3$ for the 0.75-μm and 6.4×10^6 $\mathrm{m}^2/\mathrm{m}^3$ for the 2.2-μm SiC porous structures, as listed in Table 1. These values are, respectively, 12.5 and 3.2 times larger than the corresponding geometric surface areas, clearly indicating the presence of surface roughness and microporosity in these SiC porous monoliths. Furthermore, MIP analysis of the 0.75- and 2.2-μm SiC porous structures showed a porosity of about 74%, meaning that the pressure drop across these SiC structures will be lower than that across the packed catalytic beds for the same geometric surface areas. A reliable value for the surface area of the 7.2-μm SiC porous structure could not be obtained using BET analysis because of a low surface area-to-volume ratio.

The SiC porous monoliths were coated with Ru catalyst via wet impregnation, followed by calcination in air and reduction in H_2. Ru was chosen as catalyst because of its high activity toward the decomposition of NH_3 [11,27]. The values for Ru loading as determined using inductively coupled plasma (ICP) spectrometry and dispersion of active Ru as obtained from pulsed CO and H_2 chemisorption are listed in Table 1 for the SiC porous monoliths studied here. The Ru loading and dispersion of active Ru (4.5–5.8 wt% and 20–31%, respectively) are comparable to typical values reported in the literature [27–29].

For each monolith, the surface area of active catalytic sites per gram of Ru can be derived directly from the Ru dispersion data, and the resulting values of 250–400 m^2/g are within the range of values reported in the literature for Ru/SiO_2 and Ru/Al_2O_3 [27,28]. Although the 2.2-μm SiC porous monoliths have a geometric surface area 3.2 times larger than that of the 7.2-μm SiC monoliths, the total surface area of active catalytic sites is only 1.75 times larger, indicating that the coverage of the SiC surface with Ru catalyst is not as good for the structure with smaller pore diameters. Repeated impregnation of the structures with the $RuCl_3$ solution may be required to improve the catalyst coverage on the SiC monoliths with the smaller pores.

3.2. Characterization of integrated ceramic microreactors: ammonia decomposition

3.2.1. Integrated ceramic microreactor assembly

Nondeformed and crack-free cm-scale ceramic structures with submillimeter feature sizes were obtained by modification of the drying and sintering steps of the gel-casting procedure developed previously by Young et al. for fabricating ceramic structures with much larger feature sizes [20,21]. Fig. 3a shows both optical and SEM images of a high-density, nonporous alumina structure consisting of five identical channels approximately 400 μm wide, 150 μm high, and 1 mm long, separated by 1-mm-thick walls. The Ru-coated SiC porous monoliths described in Section 3.1 are mounted in these channels using ceramic paste. A matching alumina lid with inlet and outlet tubes (Fig. 3b) is then mounted on top with ceramic paste, and an integrated ceramic microreactor is obtained after curing of the paste (Fig. 3c).

3.2.2. Ceramic microreactor testing

We characterized the performance of the integrated ceramic microreactors by studying the decomposition of NH_3 as a function of flow rate and temperature. The microreactor, 0.55 mm^3 in monolith volume, was placed in a tube furnace, and pure

Table 1
Catalyst loading and dispersion data for Ru-covered SiC porous monoliths with pore diameters of 7.2, 2.2, and 0.75 μm

Pore diameter (μm, SEM)	Surface area ($\mathrm{m}^2/\mathrm{m}^3$, BET)	Ru loading (wt%, ICP)	Ru dispersion (%, chemisorption)		Surface area of active catalytic sites per gram of Ru (m^2/g)[b]
7.2	$\sim 10^6$[a]	4.5	19.7 (CO)	20.7 (H_2)	250
2.2	6.4×10^6	5.3	29.3 (CO)	31.1 (H_2)	370
0.75	7.4×10^7	5.8	–	–	

[a] Surface area-to-volume ratio is not sufficiently large for a reliable analysis.
[b] Calculated using the Ru dispersion data obtained with CO chemisorption.

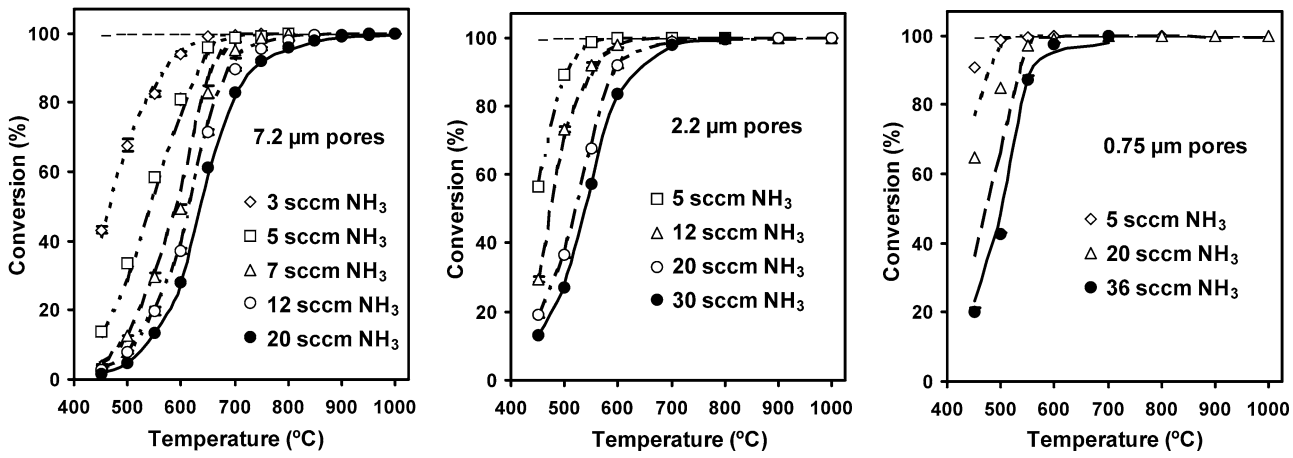

Fig. 4. NH_3 conversion using Ru-coated SiC porous monoliths (volume = 0.55 mm^3) as a function of temperature for different NH_3 flow rates measured from 450 to 1000 °C. The conversion values were obtained for integrated ceramic microreactors comprised of SiC catalytic monoliths with (a) 7.2 µm pores; (b) 2.2 µm pores; and (c) 0.75 µm pores. All data are fitted with the design equation for first-order kinetics in a PFR, assuming constant temperature and a constant pressure gradient across the reactor. (- - -) indicates the equilibrium conversion of NH_3 as a function of temperature.

NH_3 was led into the reactor through stainless steel and alumina tubing after passing through a mass flow controller. The effluent stream exited the reactor through alumina and stainless steel tubing and was led through a sampling valve for gas chromatography analysis. Fig. 4 shows the conversion of NH_3 for SiC porous monoliths with pore diameters of 7.2, 2.2, and 0.75 µm as a function of temperature over the range of 450–1000 °C for NH_3 flow rates of 3–36 sccm. The lines in the graphs are weighted least squares fits for the conversion data using first-order kinetics with respect to NH_3 in a PFR, assuming constant temperature and a constant pressure gradient across the reactor [Eq. (1), Section 2.6]. A maximum temperature drop of only 1.1 °C (endothermic reaction) can be estimated using Fourier's law of conduction for a maximum NH_3 flow rate of 36 sccm at 700 °C, justifying the assumption of constant temperature.

The fit of first-order kinetics in a PFR to the conversion data obtained with the 0.75-µm SiC porous monoliths (Fig. 4c) are poorer than those for the data obtained from the SiC monoliths with the larger pore diameters of 7.2 and 2.2 µm (Figs. 4a and 4b, respectively). The pressure drop through the 0.75-µm SiC porous monoliths is much greater than that through the 2.2- and 7.2-µm SiC monoliths and may deviate more from the calculated value obtained using the Ergun equation. In addition, the assumption of a constant pressure gradient will no longer hold for larger pressure drops across SiC monoliths with the smaller pore diameters, introducing more uncertainty into the calculated rate constants and resulting in poorer line fitting.

Fig. 4 also shows that the conversion increased with increasing temperature and with longer residence times (lower flow rates), as expected. Here, for NH_3 flow rates of 3–36 sccm, complete conversion of NH_3 (i.e., >99.9% conversion or production of 4.5–54 sccm of H_2) was reached above 700 °C, with the exact temperature at which full conversion was reached depending on the pore diameters of the SiC monoliths used in the microreactors. Although the residence time was relatively low, ranging from 0.9 to 11 ms, high conversion could still be achieved due to the high operating temperature. A maximum production of 54 sccm of H_2 corresponds to 9.8×10^4 sccm H_2 produced per cm^3 of monolith volume. Other microreactors, operating at temperatures up to 650 °C, have been reported to produce only up to $\sim 3 \times 10^3$ sccm H_2 per cm^3 of monolith or channel volume for the steam reforming of methanol [1] and the decomposition of NH_3 [12,13]. For the ceramic microreactors that we report on here, the amount of H_2 produced per cm^3 of overall reactor volume (1.05 cm^3) is 51 sccm per cm^3, a number that can be increased significantly by increasing the number of SiC catalytic monoliths within the reactors and reducing the wall thickness of the alumina housing.

The integrated ceramic microreactors showed no signs of failure after exposure to more than 15 thermal cycles of about 8 h each at temperatures as high as 1000 °C. In addition, no deactivation of catalyst was observed after exposing the reactor to 12 sccm NH_3 at 800 °C and 1000 °C for 48 h each. No conversion (i.e., <0.3%) was measured for an identical integrated ceramic microreactor without Ru catalyst when operated at 500, 800, and 1000 °C over the same range of NH_3 flow rates, indicating that the decomposition of NH_3 occurred only on the surface of the Ru catalyst deposited on the SiC porous monoliths. Thus, the rate of homogeneous decomposition of NH_3 is insignificant over the range of flow rates and resulting residence times studied here. From a ceramic material standpoint, the microreactor should be able to operate without structural degradation at temperatures up to 1200 °C in air; but to minimize the sintering of metal catalyst (here Ru), the temperature must be maintained below ~0.5 times the melting point of metal (T_m for Ru is 2600 K) [26].

3.2.3. Reaction kinetics analysis

The rate constants k' at each temperature were calculated using a weighted least squares analysis of the conversion data based on first-order kinetics with respect to NH_3 in a PFR, assuming constant temperature and a constant pressure gradi-

Table 2
Observed first-order reaction rate constants k' at different temperatures for SiC porous monoliths with pore diameters of 7.2 and 2.2 μm

	450 °C	500 °C	550 °C	600 °C	700 °C
k' (7.2 μm) in m/s	9.34×10^{-6}	7.84×10^{-6}	4.39×10^{-5}	7.23×10^{-5}	3.55×10^{-4}
k' (2.2 μm) in m/s	8.90×10^{-6}	3.01×10^{-5}	8.27×10^{-5}	1.27×10^{-4}	2.48×10^{-4}
k' (2.2 μm)/k' (7.2 μm)	0.95	3.85	1.88	1.76	0.70

ent across the reactor [23]. The value of k' calculated for the microreactor with 7.2-μm SiC porous monoliths was 4.39×10^{-5} m/s at 550 °C, and an apparent activation energy (E_a) of 22 ± 2 kcal/mol was calculated from the data acquired below 800 °C. This E_a falls within the range of values reported earlier for the decomposition of NH_3 on Ru [10,29,30]. The values of k' calculated for the microreactors with 2.2- and 0.75-μm SiC porous monoliths were 8.27×10^{-5} m/s and 5.07×10^{-5} m/s (estimated based on a 5.8 wt% Ru loading and an assumed 36% Ru dispersion for the 0.75-μm structures), respectively, at 550 °C, with activation energies of 19 ± 2 and 14 ± 2 kcal/mol.

Assuming that heat and mass transfer limitations can be neglected, the rate constant k' is only a function of the reaction temperature. Comparing the values of k' for SiC porous monoliths with pore diameters of 2.2 and 7.2 μm, however, shows that the ratio of k' values for the 2.2 μm structure and for the 7.2 μm structure changed as a function of temperature, rather than maintaining a constant value of 1 (Table 2). The data in Table 2 indicate that the k' ratio was approximately 1 at 450 °C, then increased sharply at 500 °C, and steadily decreased as the temperature increased to 650 °C, dropping to 0.70 at a temperature of 700 °C. A ratio of k' values other than 1 indicates that at a given temperature, the observed reaction rate is different for the two catalyst supports, signifying the existence of mass transfer limitations at that temperature. This trend of the changing ratio of k' values reflects that the effects of mass transfer on reaction rate predominate at higher temperatures; the diffusion coefficient of a gas increased with T^n, where n is approximately 2, whereas the reaction rate constant had an Arrhenius dependence (i.e., increased exponentially with temperature). At low temperatures, where the reactors operate in a kinetically limited regime, the k' ratio should be equal to 1. Here we obtained a k' ratio of 0.95 at 450 °C. As the temperature increases, mass transfer limitations will first affect the reaction rate for the SiC structures with a larger pore diameter (7.2 μm), and the k' ratio will increase from a value of 1, in accordance with our observations. As the temperature increases further, mass transfer limitations will control the reaction rates for both reactors, and the k' ratio will decrease until it is equal to 1. In addition, we observed a drop in the k' ratio to 0.70 at 700 °C, possibly due to invalidity of the assumption that the pressure drop gradient is constant along the length of the SiC monoliths or to deviation of the actual pressure drop from the values calculated using the Ergun equation, which was derived for a packed-bed structure, not for an inverted beaded-bed structure as used here.

From the conversion and dispersion data, we derived integral turnover frequencies (TOFs) for the SiC porous monoliths with pore diameters of 7.2 and 2.2 μm (Fig. 5). A constant TOF of about 1000 molecule/(site s) was observed for both reactors

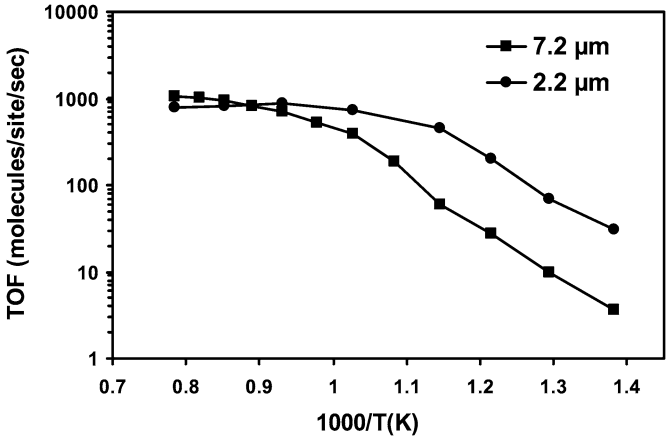

Fig. 5. Arrhenius plot of integral turnover frequencies for decomposition of NH_3 in integrated ceramic microreactors comprised of Ru-covered SiC monoliths with 7.2- and 2.2-μm pores. The lines connecting the data points are added to guide the eye.

at temperatures above 700 °C, followed by a gradual decay to lower TOF values at lower temperatures. In this lower temperature range (<700 °C), the TOFs of the SiC monoliths with 2.2-μm pore diameter were systematically higher than those of the monoliths with 7.2-μm pores. The TOF values for decomposition of NH_3 on the Ru-covered SiC porous monoliths studied here are about one order of magnitude higher than those reported by others for Ru/Al_2O_3 and Ru/SiO_2 catalysts [10,11]. This may be due to a lower metal–support interaction between the Ru catalyst and the chemically passive SiC surface [31], because previous work has shown that SiC has a lower metal–support interaction with other catalytic metals (Ni, Cu, Co, and Mo) than with SiO_2- and Al_2O_3-based supports [31,32].

4. Conclusion

We have synthesized and characterized ceramic microreactors for the on-site production of H_2. The microreactors consist of high-surface area inverted beaded SiC monoliths with 0.75-, 2.2-, or 7.2-μm interconnected pores as catalyst supports and high-density, nonporous alumina reactor housings obtained via the optimized gel-casting procedure reported here. The porous SiC monoliths have surface areas as high as 7.4×10^7 m^2/m^3, significantly higher than the geometric surface area, thus indicating the presence of surface roughness. The SiC catalyst supports are also stable at temperatures up to at least 1200 °C and have porosities up to 74%, ensuring low pressure drops across the microreactors. With an entering stream of 36 sccm NH_3, we produced up to 54 sccm of H_2 at >99.9% conversion at temperatures above 700 °C. The maximum amount of 9.8×10^4 sccm H_2 produced per cm^3 of monolith is more than

one order of magnitude higher than the hydrogen produced per cm^3 of monolith for steam reforming of methanol or decomposition of NH_3 at temperatures up to 650 °C, as reported previously [1,12,13]. Finally, using SiC as the support for Ru catalysts seems to have a beneficial effect on its catalytic performance, as evidenced by the high TOFs.

These integrated ceramic microreactors are promising for the steam reforming of higher hydrocarbons such as propane or butane. The problem of catalyst coking occurring during reforming of higher hydrocarbons below 800 °C [16] can be avoided completely by using high-temperature-compatible microreactors as described herein. This may lead to the development of microscale devices for the reforming of liquid hydrocarbons to produce H_2 on-site for use in fuel cells. Work along these lines is currently in progress. In addition, we are presently integrating a larger number of SiC monoliths within an alumina housing of similar size, to increase the hydrogen production rates per reactor volume.

Acknowledgments

This work was supported by the Department of Defense (DoD) Multidisciplinary University Research Initiative (MURI) program administered by the Army Research Office (ARO) under Contract DAAD19-01-1-0582, by the campus research board of the University of Illinois (UIUC), and by the 2004 National Research Lab Project [M 10400000061-04J0000-06110] administered by the Korean Ministry of Science and Technology. M.M. gratefully acknowledges the National Science Foundation for a graduate fellowship. Christian gratefully acknowledges support of an H.G. Drickamer Fellowship from the Department of Chemical and Biomolecular Engineering at UIUC. The SEM was carried out by UIUC's Center for Microanalysis of Materials, which is partially supported by DOE grant DEFG02-91-ER45439. Any opinions, findings, and conclusions or recommendations expressed in this publication are those of the authors and do not necessarily reflect the views of the DoD or the ARO.

References

[1] J.D. Holladay, E.O. Jones, M. Phelps, J. Hu, J. Power Sources 108 (2002) 21.
[2] D.R. Palo, J.D. Holladay, R.T. Rozmiarek, C.E. Guzman-Leong, Y. Wang, J. Hu, Y.-H. Chin, R.A. Dagle, E.G. Baker, J. Power Sources 108 (2002) 28.
[3] M.L. Perry, T.F. Fuller, J. Electrochem. Soc. 149 (2002) S59.
[4] A.S. Patil, T.G. Dubois, N. Sifer, E. Bostic, K. Gardner, M. Quah, C. Bolton, J. Power Sources 136 (2004) 220.
[5] R.R. Davda, J.A. Dumesic, Chem. Commun. (2004) 36.
[6] P. Ferreira-Aparicio, I. Rodríguez-Ramos, A. Guerrero-Ruiz, Chem. Commun. (2002) 2082.
[7] C.M. Miesse, R.I. Masel, C.D. Jensen, M.A. Shannon, M. Short, AIChE J. 50 (2004) 3206.
[8] L.R. Arana, S.B. Schaevitz, A.J. Franz, M.A. Schmidt, K.F. Jensen, J. Microelectromech. Syst. 12 (2003) 600.
[9] J.N. Armor, Appl. Catal. A 176 (1999) 159.
[10] T.V. Choudhary, C. Sivadinarayana, D.W. Goodman, Catal. Lett. 72 (2001) 197.
[11] J.C. Ganley, K.L. Riechmann, E.G. Seebauer, R.I. Masel, J. Catal. 227 (2004) 26.
[12] J.C. Ganley, E.G. Seebauer, R.I. Masel, AIChE J. 50 (2004) 829.
[13] Z. Ni, E.G. Seebauer, R.I. Masel, Ind. Eng. Chem. Res. 44 (2005) 4267.
[14] W. Wiese, B. Emonts, R. Peters, J. Power Sources 84 (1999) 187.
[15] A.V. Pattekar, M.V. Kothare, J. Microelectromech. Syst. 13 (2004) 7.
[16] J.N. Armor, D.J. Martenak, Appl. Catal. A 206 (2001) 231.
[17] I.-K. Sung, Christian, M. Mitchell, D.-P. Kim, P.J.A. Kenis, Adv. Funct. Mater. 15 (2005) 1336.
[18] D.C. Duffy, J.C. McDonald, O.J.A. Schueller, G.M. Whitesides, Anal. Chem. 70 (1998) 4974.
[19] E. Kim, Y. Xia, G.M. Whitesides, J. Am. Chem. Soc. 118 (1996) 5722.
[20] A.C. Young, O.O. Omatete, M.A. Janney, P.A. Menchhofer, J. Am. Ceram. Soc. 74 (1991) 612.
[21] O.O. Omatete, M.A. Janney, R.A. Strehlow, Am. Ceram. Soc. Bull. 70 (1991) 1641.
[22] M.A. Janney, O.O. Omatete, C.A. Walls, S.D. Nunn, R.J. Ogle, G. Westmoreland, J. Am. Ceram. Soc. 81 (1998) 581.
[23] J. Neter, W. Wasserman, M.H. Kutner, Applied Linear Statistical Models: Regression, Analysis of Variance, and Experimental Designs, Richard D. Irwin, Inc., Boston, 1990.
[24] A.S. Chellappa, C.M. Fischer, W.J. Thomson, Appl. Catal. A 227 (2002) 231.
[25] K. Tamaru, Acc. Chem. Res. 21 (1988) 88.
[26] H.S. Fogler, Elements of Chemical Reaction Engineering, Prentice Hall PTR, Upper Saddle River, 1999.
[27] X.-K. Li, W.-J. Ji, J. Zhao, S.-J. Wang, C.-T. Au, J. Catal. 236 (2005) 181.
[28] J.C. Ganley, E.G. Seebauer, R.I. Masel, J. Power Sources 137 (2004) 53.
[29] M.C.J. Bradford, P.E. Fanning, M.A. Vannice, J. Catal. 172 (1997) 479.
[30] W. Tsai, W.H. Weinberg, J. Phys. Chem. 91 (1987) 5302.
[31] M.J. Ledoux, C. Pham-Huu, Cattech 5 (2001) 226.
[32] R. Moene, E.P.A.M. Tijsen, M. Makkee, J.A. Moulijn, Appl. Catal. A 184 (1999) 127.